

Luminescence tuning of Ce³⁺, Pr³⁺ activated (Y,Gd)AGG system by band gap engineering and energy transfer

Ou, Yiyi; Zhou, Weijie; Ma, Fengkai; Liu, Chunmeng; Zhou, Rongfu; Su, Fang; Huang, Yan; Dorenbos, Pieter; Liang, Hongbin

DOI

[10.1016/j.jre.2020.01.001](https://doi.org/10.1016/j.jre.2020.01.001)

Publication date

2020

Document Version

Final published version

Published in

Journal of Rare Earths

Citation (APA)

Ou, Y., Zhou, W., Ma, F., Liu, C., Zhou, R., Su, F., Huang, Y., Dorenbos, P., & Liang, H. (2020). Luminescence tuning of Ce³⁺, Pr³⁺ activated (Y,Gd)AGG system by band gap engineering and energy transfer. *Journal of Rare Earths*, 38(5), 514-522. <https://doi.org/10.1016/j.jre.2020.01.001>

Important note

To cite this publication, please use the final published version (if applicable).
Please check the document version above.

Copyright

Other than for strictly personal use, it is not permitted to download, forward or distribute the text or part of it, without the consent of the author(s) and/or copyright holder(s), unless the work is under an open content license such as Creative Commons.

Takedown policy

Please contact us and provide details if you believe this document breaches copyrights.
We will remove access to the work immediately and investigate your claim.



Luminescence tuning of Ce³⁺, Pr³⁺ activated (Y,Gd)AGG system by band gap engineering and energy transfer[☆]

Yiyi Ou^a, Weijie Zhou^a, Fengkai Ma^a, Chunmeng Liu^a, Rongfu Zhou^a, Fang Su^a, Yan Huang^b, Pieter Dorenbos^c, Hongbin Liang^{a,*}

^a MOE Key Laboratory of Bioinorganic and Synthetic Chemistry, KLGHEI of Environment and Energy Chemistry, School of Chemistry, Sun Yat-sen University, Guangzhou 510275, China

^b Beijing Synchrotron Radiation Facility, Institute of High Energy Physics, Chinese Academy of Sciences, Beijing 100039, China

^c Faculty of Applied Sciences, Delft University of Technology, Mekelweg 15, 2629 JB, Delft, the Netherlands

ARTICLE INFO

Article history:

Received 30 October 2019

Received in revised form

26 December 2019

Accepted 2 January 2020

Available online 10 January 2020

Keywords:

Garnet

Scintillation

Band gap engineering

Energy transfer

Rare earths

ABSTRACT

Tuning of phosphor luminescence properties, including the emission energy/intensity and thermal stability, is an important way to develop superior luminescent materials for diverse applications. In this work, we discuss the effect of band gap engineering and energy transfer on the luminescence properties of Ce³⁺ or Pr³⁺ doped (Y,Gd)AGG systems, and analyze the underlying reasons for their different phenomena. By using VUV-UV excitation spectra and constructing VRBE schemes, the changes of host band structure, 5d excited level energies and emission thermal stability of Ce³⁺ and Pr³⁺ with the incorporation of Gd³⁺ ions were studied. In addition, the energy transfer dynamics was also investigated in terms of the luminescence decay curves. This work demonstrates a way to tune phosphor luminescence properties by combining band gap engineering and energy transfer tailoring and provides an inspiring discussion on the different results of Gd³⁺ doping on the Ce³⁺ and Pr³⁺ emissions.

© 2020 Chinese Society of Rare Earths. Published by Elsevier B.V. All rights reserved.

1. Introduction

Since the first investigation on Ce³⁺ doped Y₃Al₅O₁₂ (YAG) phosphor for the flying-spot cathode-ray tube (CRT) application by Blasse and Bril in 1967,¹ luminescence of lanthanide ions doped garnet systems has been studied for over fifty years. They are found to possess excellent properties of high luminous efficiency, abundant emission colors, high thermal resistance and mechanical performance. Some of the materials have been commercialized in diverse applications such as solid-state lighting, laser projection display, and near-infrared laser.^{2,3} For example, Ce³⁺ doped YAG is an efficient commercial yellow-emitting phosphor and creates the dazzling white light-emitting diodes (w-LED) when combined with (In, Ga)N blue chips.^{4,5} Lu₃Al₅O₁₂:Ce³⁺ (LuAG:Ce³⁺) shows an intense green emission with outstanding thermal stability, which makes it suitable as the green component in blue-laser-excited projection,^{6,7} Nd³⁺

doped YAG is a widely-used near-infrared (about 1.0 μm) laser source owing to its ⁴F_{3/2}-⁴I_{11/2} transition.^{8,9} In addition, due to their high light yield under high-energy radiation excitation, fast decay in the nanosecond (ns) range and easy growth of large size crystal, Ce³⁺ and Pr³⁺ activated LuAG are promising candidates for the applications in high-energy physics and medical imaging.^{10,11} Currently, to promote the materials discovery and performance improvement in lanthanide doped garnet systems, the study on the luminescence tuning of lanthanide ions (especially the Ce³⁺, Pr³⁺ and Eu²⁺ ions with 4f-5d transitions) is requisite.

In general, the adjustment of chemical composition, such as the incorporation of suitable cations or anions, is an efficient way to tune the luminescence properties of lanthanide ions with 4f-5d transitions as well as band structure of the host.¹² This adjustment relates to three aspects as follows: (i) The 4f-5d transition energies of lanthanide ions are determined by both the nephelauxetic effect (covalency or spectroscopy polarizability) and crystal field strength, which are sensitive to the change of lanthanide coordination environment induced by compositional adjustment.¹³ (ii) Because the host conduction band (CB) and valence band (VB) are formed by the electronic shells of constituent ions, band gap engineering of the host can usually be achieved by incorporation of adjusting

[☆] **Foundation item:** Project supported by the National Natural Science Foundation of China (21671201, U1632101, 61905289, 11904425) and Postdoctoral Science Foundation of China (2017M622846, 2019M663202).

* Corresponding author.

E-mail address: cesbin@mail.sysu.edu.cn (H.B. Liang).

ions.^{14,15} As a result, the thermal quenching of lanthanide 4f–5d emission can be influenced because it proceeds via thermal ionization of the 5d electron into the CB in many cases.^{16,17} In addition, the change of band structure determines the relative positions between the CB and shallow traps (usually some antisite defects), which may further influence the luminescence of samples.^{18,19} (iii) If the introduced ions have resonant energy levels, the energy transfer (ET) process between them may lead to the changes of luminescence properties, such as emission color and intensity.^{20,21} Apparently, the band gap engineering and energy transfer are important factors for the tuning of the luminous efficiency and the light yield of a series of isomorphous compounds.

Based on either band gap engineering or energy transfer, several works have shown optimization of light yield values of materials.^{22–29} However, the effect of luminescence tuning by combining these two aspects has not been well addressed so far. In this work, with the aim to systematically study the influence of band gap engineering and energy transfer on the Ce³⁺ and Pr³⁺ emissions in garnet structure, and further tuning and optimizing their luminescence properties, especially the light yield under X-ray excitation, we selected the Y₃Al₃Ga₂O₁₂ (abbreviated as YAGG hereafter) compound as the prototype host due to its suitable band gap value (about 7.31 eV) modulated by moderate Ga³⁺ substitution and good absorption of X-ray photons. By making a solid solution with Gd³⁺ ions in the YAGG host, the combination of band gap engineering and energy transfer shows a joint tuning of luminescence properties of Ce³⁺ and Pr³⁺ ions. Specifically, with the increase of Gd³⁺ content, the shifting of the energies of the Ce³⁺ excited states and the changing of Ce³⁺ and Pr³⁺ emission thermal stability were studied with VUV–UV excitation spectroscopy and constructed vacuum referred binding energy (VRBE) schemes. The energy transfer properties from Gd³⁺ to Ce³⁺ were also studied by using the Inokuti–Hirayama model to analyze the donor luminescence decay curves. Finally, X-ray excited luminescence measurements were performed to check the change of light yield of Ce³⁺ or Pr³⁺ doped (Y,Gd)AGG samples.

2. Experimental

2.1. Synthesis

A series of Y_{3–x}Ce_xAl₃Ga₂O₁₂ (YAGG:xCe³⁺) ($x = 0.005–0.05$), Y_{3–y}Gd_yAl₃Ga₂O₁₂ (YAGG:yGd³⁺) ($y = 0.15, 0.90$), Y_{2.98–y}Ce_{0.02}Gd_yAl₃Ga₂O₁₂ (YAGG:0.02Ce³⁺,yGd³⁺) ($y = 0.15–2.98$), Y_{2.99–y}Eu_{0.01}Gd_yAl₃Ga₂O₁₂ (YAGG:0.01Eu³⁺,yGd³⁺) ($y = 0–2.99$) and Y_{2.99–z}Pr_{0.01}Al₃Ga₂O₁₂ (YAGG:0.01Pr³⁺,zGd³⁺) ($z = 0–2.99$) samples were prepared via a high-temperature solid-state reaction method. The starting materials including Al₂O₃ (analytical reagent, A.R.), Ga₂O₃ (A.R.), Y₂O₃ (99.99%), CeO₂ (99.99%), Gd₂O₃ (99.99%), Eu₂O₃ (99.99%) and Pr₆O₁₁ (99.99%) were weighed stoichiometrically and ground finely in an agate mortar. The obtained homogeneous mixture was transferred into a crucible and heated at 1773 K for 8 h (for Ce³⁺/Pr³⁺ doped samples in thermal carbon reducing atmosphere while Eu³⁺/Gd³⁺ doped samples in ambient environment). After cooling to room temperature (RT), the final products were ground into powders for further characterization.

2.2. Characterization

The phase purity of synthesized samples was checked by a RIGAKU D-MAX 2200 VPC X-ray diffractometer with Cu K α ($\lambda = 0.15418$ nm) radiation at 40 kV and 26 mA. High-quality X-ray diffraction (XRD) data of the YAGG host were measured at an interval of 0.02° over a 2 θ range of 5°–110° at a Bruker D8 advance X-ray diffractometer with Cu K α ($\lambda = 0.15418$ nm) radiation at 35 kV

and 35 mA. The corresponding Rietveld refinement was performed via TOPAS-Academic software.³⁰ The morphology and elemental distribution of the synthesized host were studied on a FEI Quanta 400F scanning electron microscope (SEM) coupled with an energy dispersive spectrum (EDS) analyzer. The excitation and emission spectra in the UV–vis range and luminescence decay curves at RT were recorded on an Edinburgh FLS1000 combined fluorescence lifetime and steady-state spectrometer. The excitation source for luminescence spectra is a 450 W Xe900 xenon lamp. The sources for Ce³⁺ and Pr³⁺ decay curves in the ns region are a 150 W nF900 ns flash lamp with a pulse width of 1.0–1.6 ns and a 290 nm LED laser, respectively, while that for Gd³⁺ in the ms range is a 60 W μ F900 μ s flash lamp with a pulse width of 1.5–3.0 μ s. The excitation spectra in the VUV–UV range at 10 K were measured on the beamline 4B8 of Beijing Synchrotron Radiation Facility (BSRF), the details can be found elsewhere.^{31,32} The X-ray excited luminescence (XEL) spectra were recorded with a Philips PW2253/20 X-ray tube with a Cu anode operating at 40 kV and 25 mA at Delft University of Technology, the Netherlands.³³ The measured emission from a pressed pill of sample powder was compared with that from a pressed pill of a freshly powdered BaF₂ crystal using an equal X-ray dose during the recordings.

3. Results and discussion

3.1. Crystal structure and morphology of the YAGG host and lanthanide ions (Ce³⁺, Pr³⁺, Eu³⁺, Gd³⁺) doped samples

The crystal structure of a synthesized YAGG sample was studied by Rietveld refinement, as shown in Fig. 1(a). The obtained reliability factors ($R_{wp} = 4.75\%$, $R_p = 2.87\%$ and $R_B = 4.52\%$) imply a good fitting quality, and no impurity phase is observed. Table 1 lists the refined structural parameters. YAGG crystallizes in a cubic structure with space group *Ia-3d* (No. 230). (Fig. 1(b)).² The refined lattice constants are $a = 1.212$ nm, $V = 1.779$ nm³ and $Z = 8$. Y³⁺ ions occupy the 24c sites with eight-fold oxygen coordination in D_2 point symmetry, and the average Y³⁺–O²⁻ bond length is about 0.2375 nm, Al³⁺ and Ga³⁺ ions both occupy the 16a sites with six-fold coordination and 24d sites with four-fold coordination by certain occupation ratios as given in Table 1, respectively. The coordination environments of Y³⁺, Al³⁺ and Ga³⁺ ions are shown in Fig. 1(c). The morphology of YAGG was also investigated with SEM coupled with the EDS analyzer. The SEM image shown in Fig. S1 indicates that the sample particle has an irregular shape with a size of 10–15 μ m. The elemental mapping results show the distributions of Y, Al, Ga and O elements. Fig. 1(d) presents the XRD patterns of lanthanide doped YAGG samples at RT. They are all in line with the standard pattern of YAGG (PDF#89-6659), indicating that all samples are of the same pure phase of YAGG. The incorporation of lanthanide ions does not significantly influence the crystal structure. Since the doped lanthanide ions have similar ionic radii [$r(\text{Ce}^{3+}) = 0.1143$ nm, $r(\text{Pr}^{3+}) = 0.1126$ nm, $r(\text{Eu}^{3+}) = 0.1066$ nm, $r(\text{Gd}^{3+}) = 0.1053$ nm] with Y³⁺ ions [$r(\text{Y}^{3+}) = 0.1019$ nm] for 8-fold coordination,³⁴ they are expected to enter the Y³⁺ sites.

3.2. Luminescence of Ce³⁺ and construction of VRBE schemes

The highest-height normalized excitation ($\lambda_{em} = 529$ nm) and emission ($\lambda_{ex} = 435$ nm) spectra of sample YAGG:0.005Ce³⁺ at RT are shown in Fig. 2(a). Upon 435 nm excitation, the emission spectrum presents a broad band in the green-yellow region peaking at about 529 nm. It is fitted by using two-Gaussian-functions in Fig. S2. The transition energies from the lowest 5d state (5d₁) to the ²F_{5/2} and ²F_{7/2} 4f ground states can be estimated to be about 2.40

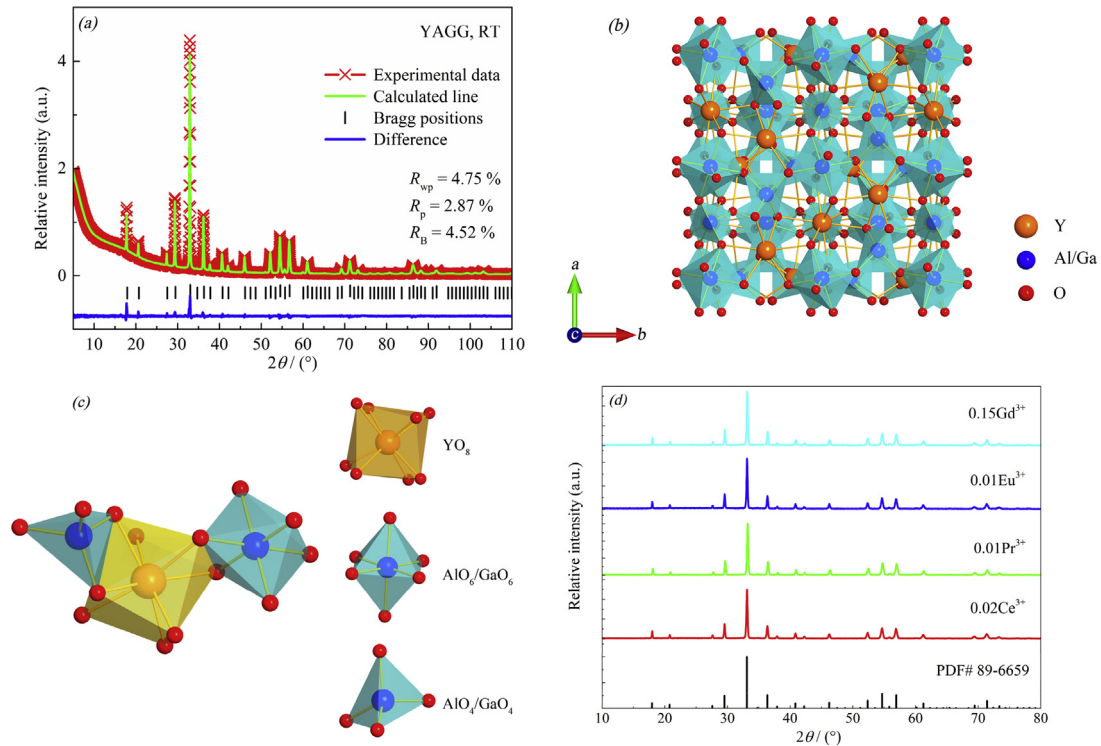


Fig. 1. (a) Rietveld refinement of laboratory XRD data of the undoped YAGG at RT; (b) Crystal structure of YAGG viewed along *c* axis; (c) Coordination polyhedra of Y^{3+} , Al^{3+} and Ga^{3+} ions; (d) XRD patterns of YAGG:0.02 Ce^{3+} /0.01 Pr^{3+} /0.01 Eu^{3+} /0.15 Gd^{3+} at RT.

Table 1
Refined structural parameters of YAGG^a at RT.

Site	Wyck.	<i>x</i>	<i>y</i>	<i>z</i>	Occ.	<i>B</i> _{iso}
Y	24c	0.125	0	0.125	1	1.0429
Al1	16a	0	0	0	0.7147	1.5466
Ga1	16a	0	0	0	0.2853	1.2720
Al2	24d	0.375	0	0.25	0.5156	1.5466
Ga2	24d	0.375	0	0.25	0.4844	1.2720
O1	96h	-0.0271	0.0500	0.1504	1	1.6802

^a Symmetry, cubic; space group, *Ia-3d*; *a* = 1.212 nm, *V* = 1.779 nm³, *Z* = 8; weighted-profile agreement index, *R*_{wp} = 4.75%; profile residual agreement index, *R*_p = 2.87%; Bragg-intensity agreement index, *R*_B = 4.52%.

and 2.14 eV, respectively. The decay curve of Ce^{3+} emission is single-exponential with a lifetime of about 68.9 ns, as shown in the inset of Fig. 2(a). When monitoring the Ce^{3+} emission at 529 nm, the excitation spectrum in the UV range exhibits two bands located at about 347 nm (3.57 eV) and 435 nm (2.84 eV), which are attributed to the transitions from the Ce^{3+} 4f ground states to the crystal-field-split 5d₂ and 5d₁ excited states, respectively. These results are in accordance with those reported in the literature,^{35,36} although the energy of the 5d₁ excited state seems a little bit larger than that (\approx 2.78 eV) compiled in Ref. ³⁷. This may be due to the uncertainty of volatile Ga^{3+} amount in the samples or experimental errors in the spectral collection. To study the other three 5d excitation bands of Ce^{3+} ions in YAGG, we collected its VUV-UV excitation spectrum in a wavelength range of 125–360 nm by using the BSRF VUV light source as presented in Fig. 2(b). The spectral profile in the range of 3.44–3.87 eV (320–360 nm) is consistent with those in the UV excitation spectrum. The VUV-UV excitation spectrum exhibits two broad bands in the higher energy side. The band peaked at about 6.93 eV (\approx 179 nm) is assigned to the host exciton

absorption band, thus the corresponding exciton creation energy (E^{ex}) is 6.93 eV. The band gap (E_g) of YAGG is estimated as about 7.31 eV after adding the exciton binding energy [0.008 \times (E^{ex})² = 0.38 eV].³⁸ The band at about 5.46 eV (\approx 227 nm) is then the superposition of the three 4f \rightarrow 5d_{3,4,5} excitation bands. Such overlapping of Ce^{3+} 5d excitation bands is normal for Ce^{3+} -doped garnet phosphors due to the octahedral coordination environment with an additional tetragonal distortion.^{37,39} With the aim to further determine the energetic positions of these three higher 5d excitation bands, we fitted the excitation spectrum in the range of 4.51–5.85 eV (275–212 nm) by three Gaussian functions.³⁹ The results in Fig. S3 show their band energies at about 5.02, 5.37 and 5.74 eV, respectively. With these assignments, the centroid energy or arithmetic mean of the five Ce^{3+} 4f-5d energies is about 4.51 eV. The centroid shift (ϵ_c), i.e., the energy decrease of the Ce^{3+} 5d centroid in YAGG relative to that of free Ce^{3+} ions (6.35 eV), is about 1.84 eV. The crystal field splitting (ϵ_{cfs}) defined as the energy difference between the Ce^{3+} 5d₁ and 5d₅ states is estimated to be about 2.88 eV. The Stokes shift of Ce^{3+} emission is about 0.44 eV as obtained from the energy difference between the 5d₁ excitation band and 5d₁ \rightarrow ²F_{5/2} emission band. All of these results on the energies of Ce^{3+} 5d excited states are similar to those reported in other works.³⁹

By using the centroid shift energy (1.84 eV), the band gap value (7.31 eV), along with the charge transfer (CT) energy of Eu^{3+} in YAGG (\approx 5.21 eV, see Fig. S4), we constructed the vacuum referred binding energy (VRBE) scheme of lanthanide ions in YAGG using the chemical shift method.⁴⁰ The result in Fig. 2(c) can be used to explain many important luminescence properties of lanthanide ion doped phosphors including the thermal quenching of Ce^{3+} 5d-4f emission, valence stability of doped ions and the electron/hole trap depths, and so on.^{17,41,42} In our case, the energy difference E_{dc} between the Ce^{3+} 5d₁ state and the bottom of conduction band is read

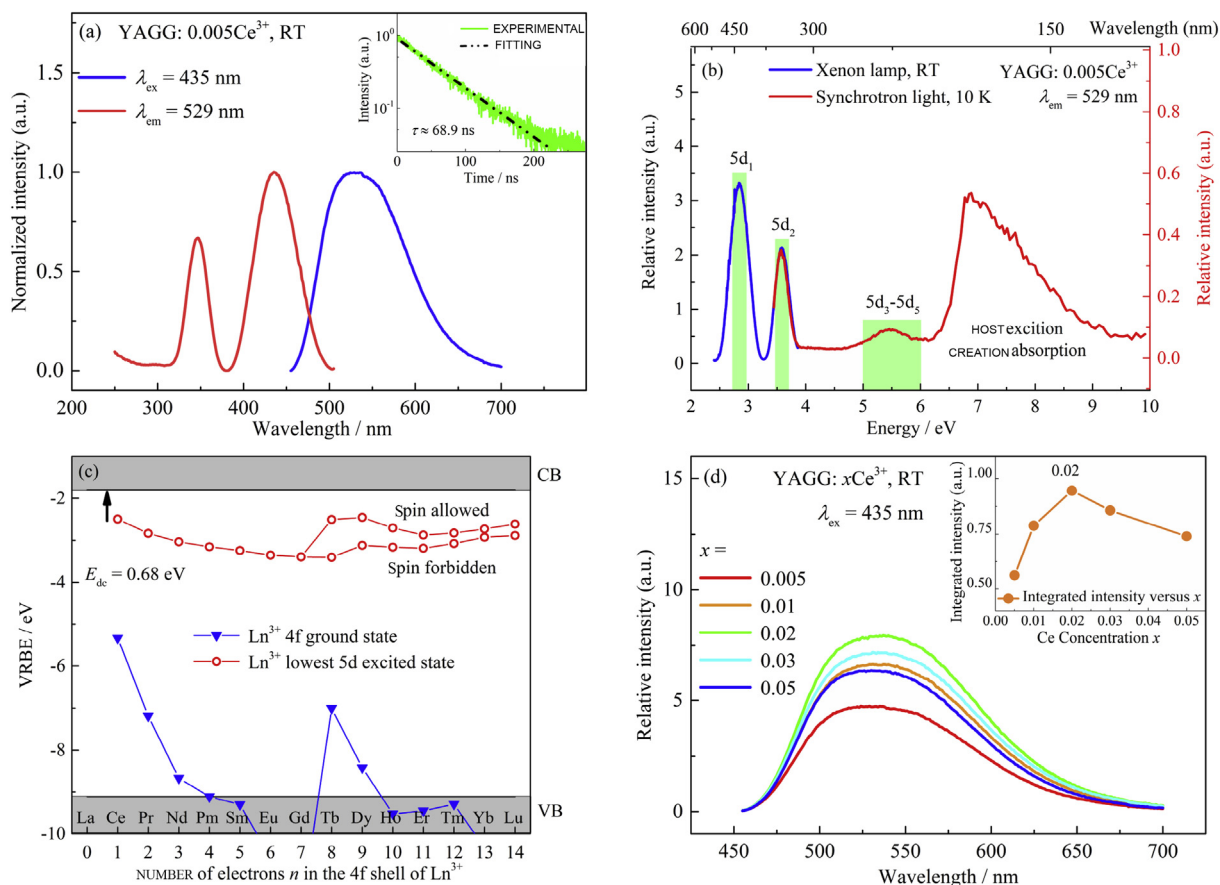


Fig. 2. (a) Highest-height normalized excitation ($\lambda_{em} = 529$ nm) and emission ($\lambda_{ex} = 435$ nm) spectra of sample YAGG:0.005Ce³⁺ at RT. The inset displays the decay curve of Ce³⁺ emission ($\lambda_{ex} = 435$ nm, $\lambda_{em} = 529$ nm); (b) VUV-UV and UV excitation spectra ($\lambda_{em} = 529$ nm) of sample YAGG:0.005Ce³⁺ collected by using BSRF VUV light at 10 K and laboratory xenon lamp at RT, respectively; (c) VRBE scheme of lanthanide ions in the YAGG host; (d) Concentration-dependent emission ($\lambda_{ex} = 435$ nm) spectra of samples YAGG:xCe³⁺ ($x = 0.005$ – 0.05) at RT. The inset shows the integrated intensity as a function of Ce³⁺ concentration.

as about 0.68 eV from Fig. 2(c), which indicates that the emission of Ce³⁺ doped YAGG phosphor may possess a moderate thermal stability.^{16,37}

Concentration-dependent luminescence properties of Ce³⁺-doped samples are shown in Fig. 2(d). The integrated emission intensity has a maximum when $x = 0.02$, which indicates that concentration quenching occurs in the higher concentration range. We therefore selected the sample YAGG:0.02Ce³⁺ to investigate its radioluminescence properties. Fig. 3 shows its X-ray excited luminescence spectrum together with that of the BaF₂ reference sample at RT. The emission curve of BaF₂ presents two bands with maxima at about 228 and 310 nm, which are ascribed to the core valence luminescence and self-trapped-exciton (STE) emission, respectively.⁴³ For sample YAGG:0.02Ce³⁺, its emission profile and position under X-ray excitation are consistent with the results under UV excitation discussed above and its absolute scintillation light yield is estimated to be 5400 ± 1400 ph/MeV based on the ratio of its integrated intensity with that of the BaF₂ (≈ 8880 ph/MeV) reference. As a matter of fact, the fundamental limit of X-ray excited luminescence of YAGG:Ce³⁺ system would be beyond 50000 ph/MeV.¹⁰ In our case, only about 5000 ph/MeV value was collected, which indicates that most of the energies of free electrons and holes created by X-ray excitation failed to be captured by the Ce³⁺ ions. In the following section, we will apply two aspects, i.e., band gap engineering and energy transfer tailoring, to tune the radioluminescence light yields of Ce³⁺ doped (Y,Gd)AGG phosphors by making a solid solution with Gd³⁺ ions in the YAGG host.

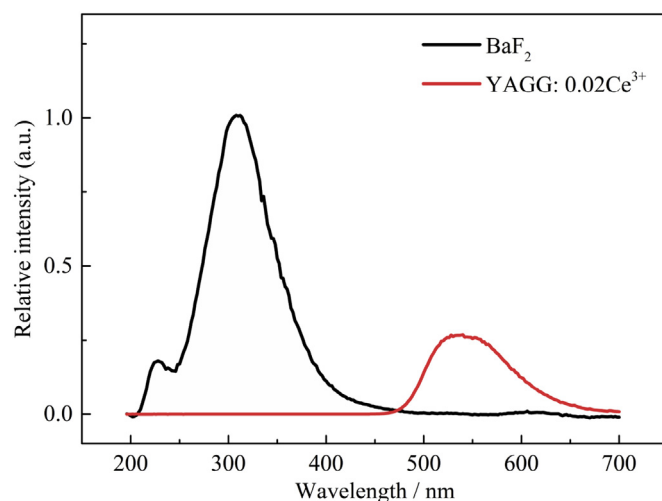


Fig. 3. X-ray excited luminescence spectra of sample YAGG:0.02Ce³⁺ and the BaF₂ reference at RT.

3.3. Influence of Gd³⁺ incorporation on luminescence of Ce³⁺

Fig. 4(a) shows the VUV-UV and UV excitation ($\lambda_{em} = 529, 539, 558, 568$ nm) spectra of samples YAGG:0.02Ce³⁺_yGd³⁺ ($y = 0$ – 2.98) by using the BSRF VUV light source and the laboratory

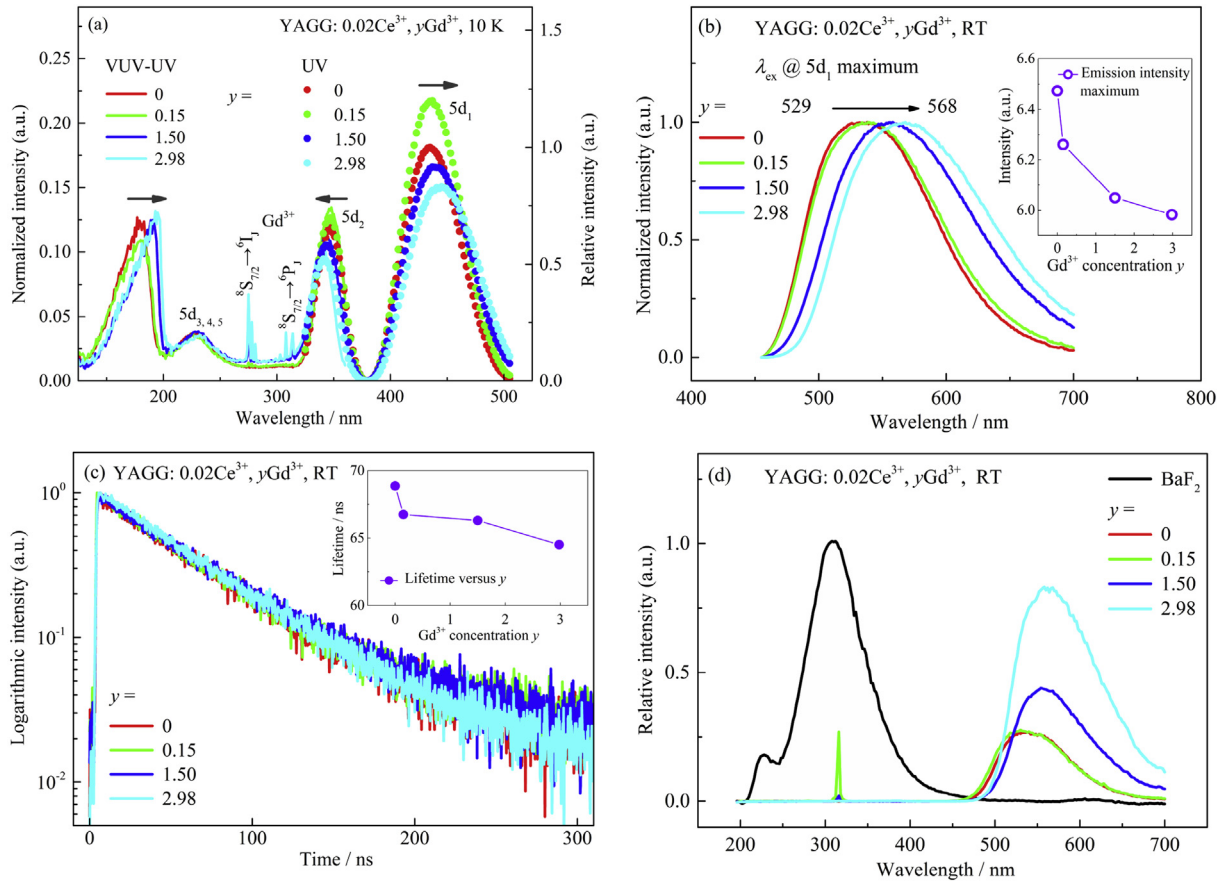


Fig. 4. (a) VUV-UV excitation ($\lambda_{em} = 529, 539, 558, 568$ nm) spectra of samples YAGG:0.02Ce³⁺,yGd³⁺ ($y = 0, 0.15, 1.50, 2.98$) by using the BSRF VUV light source and the laboratory xenon lamp; (b) Highest-height normalized emission ($\lambda_{ex} = 435, 438, 440, 446$ nm) spectra at RT, the inset shows the concentration-dependent peak emission intensity; (c) Luminescence decay curves [$\lambda_{ex} = 435$ nm, $\lambda_{em} = 529$ nm ($y = 0$); $\lambda_{ex} = 438$ nm, $\lambda_{em} = 539$ nm ($y = 0.15$); $\lambda_{ex} = 440$ nm, $\lambda_{em} = 558$ nm ($y = 1.50$); $\lambda_{ex} = 446$ nm, $\lambda_{em} = 568$ nm ($y = 2.98$)] at RT; (d) X-ray excited luminescence spectra at RT.

xenon lamp, respectively. The area-normalized VUV-UV excitation profiles coincide well with the UV excitation profiles in the wavelength range of 325–360 nm. With the increase of Gd³⁺ concentration, the host exciton absorption band shifts from 179 to 195 nm, which indicates that the band gap of (Y,Gd)AGG solid solution becomes smaller as listed in Table 2. The sharp excitation lines in the wavelength range of 275–315 nm are due to the 4f-4f transitions ($^8S_{7/2} \rightarrow ^6I_J, ^6P_J$) of Gd³⁺ ions and become more pronounced when Gd³⁺ concentration increases. This demonstrates that energy transfer from Gd³⁺ to Ce³⁺ takes place. The 5d₁ excitation band of Ce³⁺ shifts from 435 to 446 nm while the 5d₂ excitation band

moves in an opposite direction from 347 to 342 nm. The broad band originating from the three higher 5d_{3, 4, 5} bands seems stable, which is well in line with the results reported elsewhere.^{44,45} The changing 5d excitation bands are caused by a combination of nephelauxetic effect (covalence or spectroscopic polarizability) and crystal field strength due to the Gd³⁺ incorporation.^{39,46} Fig. 4(b) presents the highest-height normalized emission spectra under the excitation of the Ce³⁺ 5d₁ band. The emission band red-shifts from 529 to 568 nm, which is caused by the red-shift of the 5d₁ excitation band, the increased Stokes shift of Ce³⁺ emission, and band broadening induced by the presence of distorted Ce³⁺ sites. From the Ce³⁺ spectral data compiled in Table 2, the 5d₁ excitation band red-shifts by about 0.07 eV and it plays a primary role in pushing the Ce³⁺ emission to longer wavelengths. The inset of Fig. 4(b) shows that with the increase of Gd³⁺ concentration, the intensity of Ce³⁺ emission gradually decreases regardless of the constant nominal content of Ce³⁺ ions (about 0.02). We think that it is mainly due to the increased thermal quenching caused by the narrowing of the host band gap. This is supported by the slight decrease of average Ce³⁺ emission lifetime values as presented in Fig. 4(c). A detailed discussion will be given later.

Finally, the X-ray excited luminescence of samples YAGG:0.02Ce³⁺,yGd³⁺ ($y = 0–2.98$) was studied (see Fig. 4(d)). The X-ray excited emission spectra shift to longer wavelengths with increase of Gd³⁺ content. This is similar to the spectra under the excitation of the 5d₁ state as shown in Fig. 4(b). Remarkably, these samples show enhanced Ce³⁺ X-ray excited emission with

Table 2

Gd³⁺-concentration-dependent band gap (E_g) values of the hosts, 5d excitation bands (5d₁, 5d₂) of Ce³⁺ and charge transfer bands of Eu³⁺.

Gd ³⁺ content	HEA ^a (nm)	E_g^b (eV)	λ_{ex}^c (nm)		λ_{em}^d (nm)	E_{CT}^e (nm)
			5d ₁	5d ₂		
0	179	7.31	435	347	529	238
0.15	181	7.23	438	346	539	240
1.50	190	6.86	440	344	558	242
2.98	195	6.68	446	342	568	244

^a Host exciton absorption band.

^b Host band gap.

^c The 5d₁ and 5d₂ excitation bands of Ce³⁺.

^d Emission bands of Ce³⁺.

^e Charge transfer bands of Eu³⁺.

increasing Gd^{3+} content. The corresponding absolute light yield values are compiled in Table 3. The sample ($y = 2.98$) with full Gd^{3+} replacing of Y^{3+} shows a light yield of 10000 ± 700 ph/MeV, which is nearly twice of the sample without Gd^{3+} .

Consequently, the Gd^{3+} incorporation is found helpful to improve the light yield of Ce^{3+} ions in YAGG. In fact, with the increase of Gd^{3+} ions, the induced band gap narrowing and the interaction between Gd^{3+} and Ce^{3+} mainly modulate the thermal stability of Ce^{3+} emission and ET process from Gd^{3+} to Ce^{3+} , which eventually influences the Ce^{3+} radioluminescence to a large extent. We will then discuss the roles of these two facets in detail.

3.3.1. Band gap narrowing and thermal stability of Ce^{3+} emission

As discussed in Fig. 4(a), with the increase of Gd^{3+} concentration, the band gap of (Y,Gd)AGG turns smaller, and the Ce^{3+} 5d excited states ($5d_1$ and $5d_2$) show gradual changes. When Eu^{3+} ions are incorporated, the charge transfer band also presents a red-shift from 238 to 244 nm as shown in Fig. S4 and Table 2, which is consistent with the results reported elsewhere.^{47,48} With the aim to study the influence of band gap narrowing on the emission properties of Ce^{3+} , especially the thermal stability, we constructed the VRBE schemes for lanthanide ions in the (Y,Gd)AGG systems. The required band gap values, Eu^{3+} charge transfer bands, the energies of the first two 5d excited levels ($5d_1$ and $5d_2$) as read from Fig. 4(a) are compiled in Table 2. As for the higher three 5d levels, their superposition bands in the region of 212–273 nm in Fig. S5 seem quite stable throughout the Gd^{3+} concentration range. Consequently, we assume that the higher 5d levels stay unchanged with the incorporation of Gd^{3+} and use the higher three 5d excited state energies of Ce^{3+} in YAGG (see Fig. S5) to represent those in the (Y,Gd)AGG systems for the construction of VRBE schemes (see Fig. S6).

The vacuum referred binding energies at the top of the host valence band and conduction band bottom, and that of the Ce^{3+} 4f and 5d levels are extracted from the VRBE schemes and shown in Fig. 5 and Table 4 for clear comparisons. With the increase of Gd^{3+} , the bottom of the CB lowers from about -1.80 to -2.30 eV. The top of the VB that is formed by the oxygen 2p-shell electrons appears relatively stable. Consequently, the lowering of the CB bottom causes the narrowing of the band gap. As for the Ce^{3+} energy levels, due to the similar Coulomb repulsion effect from the screening charge of the anions based on the chemical shift model,³⁶ the VRBE of 4f ground state appears quite constant (≈ 5.33 eV). But the VRBE of the $5d_1$ excited state decreases because of larger crystal field splitting. The energy gap E_{dc} between the Ce^{3+} $5d_1$ excited state and the bottom of CB for different Gd^{3+} content is collected in Fig. 5. The E_{dc} value decreases from about 0.68 to 0.25 eV, implying that Ce^{3+} emission thermal quenching via thermal ionization of the 5d electron to the CB may happen at lower temperature and the corresponding thermal stability gets poor. The decreases of Ce^{3+} emission intensity (Fig. 4(b)) and lifetime value (Fig. 4(c)) at RT with the increase of Gd^{3+} concentration as discussed above support this judgement. Consequently, from the viewpoint of thermal quenching of Ce^{3+} emission, the band gap narrowing induced by the Gd^{3+} incorporation is not helpful to improve the luminescence efficiency of Ce^{3+} ions. However, the depressing of CB bottom in this work

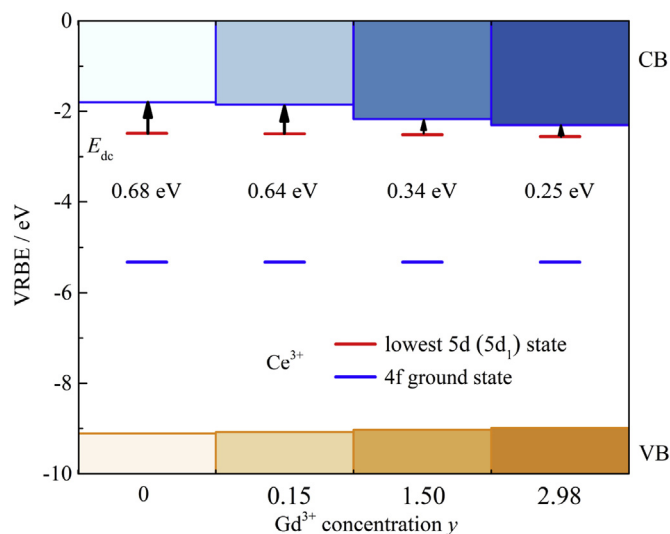


Fig. 5. Schematic diagram of vacuum referred binding energies of valence/conduction bands and Ce^{3+} 4f ground and $5d_1$ excited states in YAGG:0.02 Ce^{3+} $_y\text{Gd}^{3+}$ ($y = 0$ –2.98) systems.

may also positively affect the scintillator performance of samples via overlapping the shallow traps (usually the antisite defects in YAG-type host) near the CB bottom and improving the sensitization of Ce^{3+} ions by free electron and holes under X-ray excitation.^{18,19,22,23}

3.3.2. Energy transfer dynamics from Gd^{3+} to Ce^{3+}

As discussed above, Fig. 4(a) shows the sharp $^8\text{S}_{7/2} \rightarrow ^6\text{P}_j$, $^6\text{I}_j$ lines of Gd^{3+} in the excitation spectra of samples YAGG:0.02 Ce^{3+} $_y\text{Gd}^{3+}$ ($y = 0.15$ –2.98) by monitoring Ce^{3+} emission, which indicates that there exists energy transfer (ET) from Gd^{3+} to Ce^{3+} . Fig. 6(a) presents the emission spectra of YAGG:0.02 Ce^{3+} $_y\text{Gd}^{3+}$ ($y = 0.15$ –2.98) at RT under excitation of Gd^{3+} at 275 nm. With the increase of Gd^{3+} content, the $^6\text{P}_j \rightarrow ^8\text{S}_{7/2}$ Gd^{3+} emission at about 314 nm turns weaker, while the Ce^{3+} emission at 475–700 nm becomes stronger with a red-shifting that is similar to the results in Fig. 4(b). These phenomena evidence ET from Gd^{3+} to Ce^{3+} and reveal the sensitizing role of donor Gd^{3+} on the enhancement of acceptor Ce^{3+} emission under UV excitation. When excited by X-ray, this sensitizing effect keeps working and the ET from Gd^{3+} to Ce^{3+} plays a positive role in increasing the light yield of samples YAGG: 0.02 Ce^{3+} $_y\text{Gd}^{3+}$ as presented in Fig. 4(d). At the same time, the incorporation of Gd^{3+} ions can also capture the energies of free electrons and holes of materials under X-ray excitation.

To get deeper insight into the ET dynamics from Gd^{3+} to Ce^{3+} , we collected the luminescence decay curves ($\lambda_{\text{ex}} = 275$ nm, $\lambda_{\text{em}} = 314$ nm) of donor Gd^{3+} ions in the samples YAGG: $y\text{Gd}^{3+}$ ($y = 0.15, 0.90$) and YAGG:0.02 Ce^{3+} $_y\text{Gd}^{3+}$ ($y = 0.15, 0.90$) as depicted in Fig. 6(b), respectively. In the YAGG: $y\text{Gd}^{3+}$ samples, the decay profile of Gd^{3+} ions at diluted scenario ($y = 0.15$) is single-exponential, indicating that concentration quenching of Gd^{3+} emission does not yet happen and that the Gd^{3+} ions are isolated from each other. The radiative lifetime of Gd^{3+} emission is about 3.22 ms. With the increase of Gd^{3+} content to $y = 0.90$, the decay curve deviates from single-exponential, which implies that concentration quenching occurs and that ET between Gd^{3+} ions becomes active. Sample YAGG:0.02 Ce^{3+} $_{0.15}\text{Gd}^{3+}$ shows a luminescence curve with faster decay compared with that of sample YAGG:0.15 Gd^{3+} with the same Gd^{3+} content. It is due to the activation of a Gd^{3+} depopulation path via the energy transfer from

Table 3
Light yield of YAGG:0.02 Ce^{3+} $_y\text{Gd}^{3+}$ ($y = 0$ –2.98).

Gd^{3+} content	Light yield (ph/MeV)
0	5400 ± 1400
0.15	5100 ± 1000
1.50	5900 ± 700
2.98	$10,000 \pm 700$

Table 4
Vacuum referred binding energies of valence band (VB) top, conduction band (CB) bottom, Ce³⁺ 4f ground and 5d₁ excited states in YAGG:0.02Ce³⁺,yGd³⁺ (y = 0–2.98) systems.

Gd ³⁺ content	VB top (eV)	CB bottom (eV)	Ce ³⁺ 4f ground state (eV)	Ce ³⁺ 5d ₁ excited state (eV)	E _{dc} (eV)
0	-9.11	-1.80	-5.33	-2.48	0.68
0.15	-9.08	-1.85	-5.33	-2.49	0.64
1.50	-9.03	-2.17	-5.33	-2.51	0.34
2.98	-8.99	-2.30	-5.33	-2.55	0.25

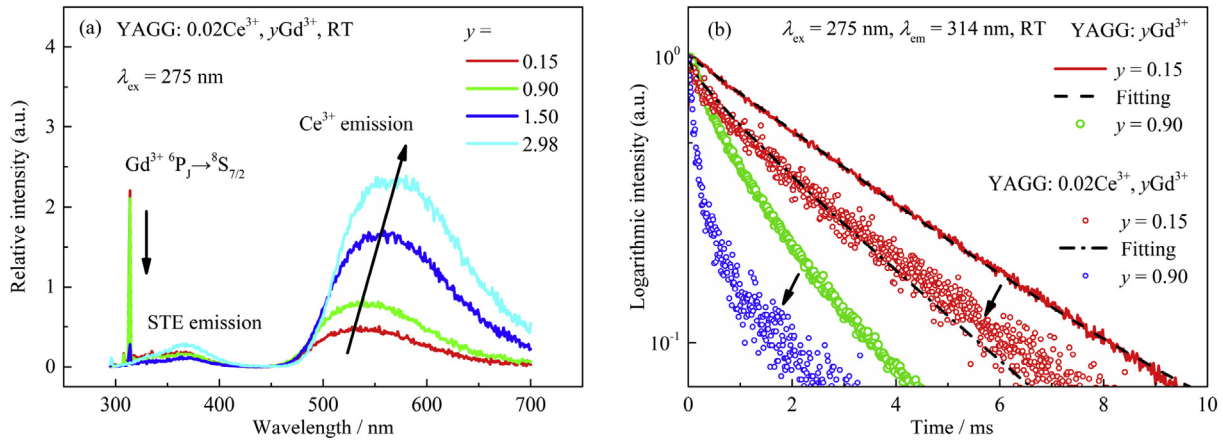


Fig. 6. (a) Emission ($\lambda_{\text{ex}} = 275$ nm) spectra of samples YAGG:0.02Ce³⁺,yGd³⁺ (y = 0.15–2.98) at RT; (b) Luminescence decay curves ($\lambda_{\text{ex}} = 275$ nm, $\lambda_{\text{em}} = 314$ nm) of samples YAGG:yGd³⁺ (y = 0.15, 0.90) and YAGG:0.02Ce³⁺,yGd³⁺ (y = 0.15, 0.90) at RT and fitting results via Inokuti-Hirayama ET model.

Gd³⁺ to Ce³⁺. Considering that the Gd³⁺ ions are isolated from each other at the content of y = 0.15, the donor Gd³⁺ ions transfer the energy to acceptor Ce³⁺ without energy migration between Gd³⁺ ions. For this scenario, the Inokuti-Hirayama ET model⁴⁹ established on the assumptions of (i) the spherically continuous distribution of acceptor around isolated donor and (ii) the inverse power relation between energy transfer rate and distance for multipolar interaction cases can be used to describe the luminescence decay curves of donor Gd³⁺ ions as given below:

$$\frac{I(t)}{I(0)} = \exp \left[- \left(\frac{t}{\tau_0} \right) - \frac{4\pi}{3} C_A \Gamma \left(1 - \frac{3}{S} \right) (C_{DA})^{3/S} t^{3/S} \right] \quad (1)$$

where $I(t)$ and $I(0)$ represent the emission intensities of Gd³⁺ emission at time t and initial time, respectively. τ_0 is the intrinsic lifetime of donor Gd³⁺ emission (≈ 3.22 ms, Fig. 6(b)), C_A is the concentration of Ce³⁺ acceptor, $\Gamma(1-3/S)$ is the gamma function and the S value indicates the type of multipolar interaction type between donor and acceptor [i.e., 6 for electric dipole–dipole interaction (EDD), 8 for electric dipole–quadrupole (EDQ) and 10 for electric quadrupole–quadrupole (EQQ)]. C_{DA} is the ET microparameter. When we set $S = 6$, the best fitting quality can be achieved as shown in Fig. 6(b). Consequently, the main mechanism of ET from Gd³⁺ to Ce³⁺ ions is electric dipole–dipole interaction and the ET microparameter C_{DA} is fitted to be about 1.272×10^{-52} m⁶/s with the fitting quality coefficient $R_{\text{adj}}^2 = 0.9898$. For the sample YAGG:0.02Ce³⁺,0.90Gd³⁺, the energy transfer rate from Gd³⁺ to Ce³⁺ becomes higher, which causes that the luminescence decay curve drops more rapidly than that of sample YAGG:0.90Gd³⁺ with the same Gd³⁺ concentration. The energy transfer from Gd³⁺ to Ce³⁺ in this concentrated case is more complicated with the involvement of energy migration between Gd³⁺ as discussed above. In addition, the heavy doping of Gd³⁺ also severely shortens the distance between Gd³⁺ ions, which may lead to the activation of energy transfer between Gd³⁺–Ce³⁺ and Gd³⁺–Gd³⁺ pairs via other

short-range interaction mechanisms, such as electric dipole–quadrupole (EDQ) or electric quadrupole–quadrupole (EQQ) interaction as mentioned above.

3.4. Influence of Gd³⁺ incorporation on luminescence of Pr³⁺

We also studied the luminescence properties of Pr³⁺ ions in YAGG host and the corresponding effect of Gd³⁺ incorporation. Fig. 7 shows the excitation, emission spectra as well as the luminescence decay curve of sample YAGG:0.01Pr³⁺. As can be seen in Fig. 7(a), the broad excitation band located at about 282 nm is assigned to the 4f–5d excitation band of Pr³⁺ ions, whose energy is about 1.52 eV higher than the lowest excited band of Ce³⁺.⁵⁰ In the emission profile of Pr³⁺ ions, the broad bands in the wavelength range of 300–450 nm can be attributed to the transitions from the 5d excited state to 4f states (³H_{*J*} (*J*=4–6), ³F_{*J*} (*J*=2–4)); while the sharp peaks at the region of 450–700 nm are attributed to 4f–4f transitions.⁵¹ Fig. 7(b) displays the luminescence decay curve of Pr³⁺ f–d transition and its lifetime is estimated to be about 12.3 ns; the results for luminescence decay curves of ³P₀–³H₄ and ¹D₂–³H₄ transitions are also fitted to be about 19.8 and 139.8 μ s, respectively (Fig. S7).

To study the effect of Gd³⁺ incorporation on the luminescence properties of Pr³⁺ ions, the XEL spectra of YAGG:0.01Pr³⁺,zGd³⁺ (z = 0, 1.50, 2.99) were also recorded at RT (Fig. 8). Due to the similarity of the influence of coordination environment on 4f–5d transitions,⁵² the incorporation of Gd³⁺ may also induce the change of 5d transition energies of Pr³⁺ ions and the band gap narrowing of host, which is like the results of Ce³⁺ ions in Fig. 4(a). However, the XEL results of Pr³⁺ ions in Fig. 8 is quite different from that of Ce³⁺ in Fig. 4(d). With the increase of Gd³⁺ content, the 4f–5d emission of Pr³⁺ ions gradually decreases, which finally results in the degradation of absolute light yield values from about 3600 to 1600 ph/MeV as listed in Table 5. Since the lowest 5d excited states of Pr³⁺ are farther from the CB bottom of host compared with Ce³⁺ case, as

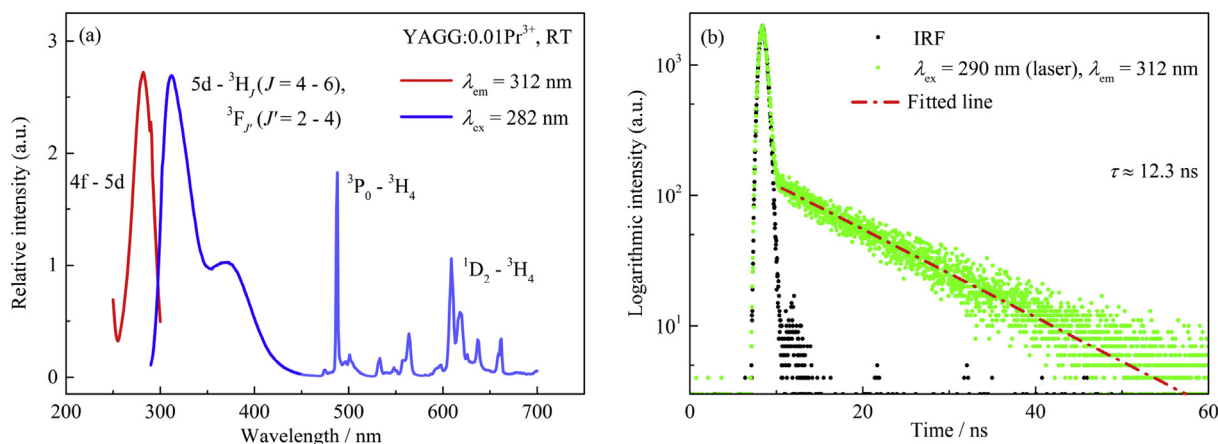


Fig. 7. (a) Excitation ($\lambda_{em} = 312$ nm) and emission ($\lambda_{ex} = 282$ nm) spectra of sample YAGG:0.01Pr³⁺ at RT; (b) Luminescence decay curve ($\lambda_{ex} = 290$ nm, $\lambda_{em} = 312$ nm) of sample YAGG:0.01Pr³⁺ at RT.

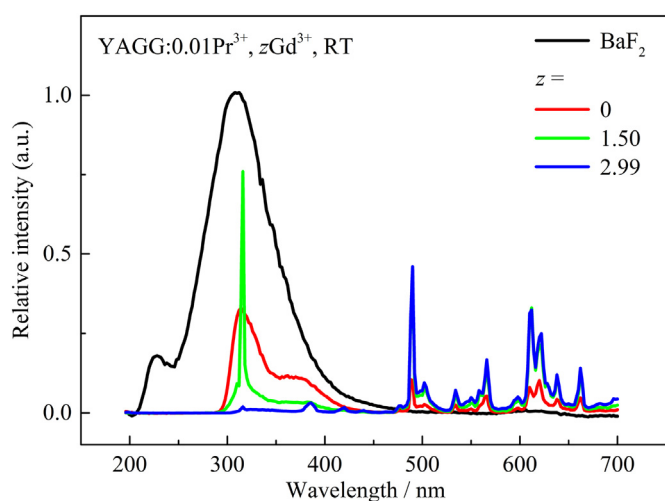


Fig. 8. The X-ray luminescence (XEL) spectra of samples YAGG:0.01Pr³⁺, zGd³⁺ ($z = 0, 1.50, 2.99$) and BaF₂ reference at RT.

Table 5
Light yield of YAGG:0.01Pr³⁺, zGd³⁺ ($z = 0, 1.50, 2.99$).

Gd ³⁺ content	Light yield (ph/MeV)
0	3600 ± 700
1.50	2800 ± 1000
2.98	1600 ± 600

indicated by the large average E_{dc} (≈ 0.82 eV) obtained in VRBE schemes (Fig. S6), the Gd³⁺-induced band gap narrowing actually does not have significant impact on the thermal-quenching of Pr³⁺ 5d-4f luminescence. We therefore assume that the complex energy transfer between 5d and 4f states of Pr³⁺ and 4f states of Gd³⁺ will play an important role in decreasing the Pr³⁺ emission, except for the effect of other defects on the XEL light yields of three cases.⁵³ This intricate issue will be further discussed in detail in future.

4. Conclusions

In summary, the influences of band gap engineering and energy transfer on the luminescence properties of Ce³⁺ or Pr³⁺ doped (Y,Gd)AGG phosphors were studied in this work. With increasing

Gd³⁺ content in the YAGG host, the VUV-UV excitation spectra show that the band gap gets smaller, and the Ce³⁺ 5d₁ excitation band red-shifts from 435 to 446 nm, while 5d₂ band shows a blue-shifting from 347 to 342 nm. The superposition of the three higher 5d (5d_{3,4,5}) bands stay almost unchanged. These evolutions of Ce³⁺ 5d excited levels were collectively determined by the nephelauxetic effect (covalency or spectroscopy polarizability) and crystal field strength of the Ce³⁺ site environment modulated by Gd³⁺ incorporation. The Ce³⁺ emission bands also present a red-shifting from 529 to 568 nm, which is mainly due to the depressing of 5d₁ excited level. The constructed VRBE schemes further demonstrate that the narrowing of host band gap is primarily caused by the lowering of the bottom of the conduction band, which also decreases the energy gap between the Ce³⁺ 5d₁ level and the bottom of the CB and may lead to the degradation of Ce³⁺ emission thermal stability. Moreover, the incorporation of Gd³⁺ ions also sensitizes the luminescence of Ce³⁺. By applying the Inokuti-Hirayama model to analyze the luminescence decay curves of donor Gd³⁺ emission, the main interaction mechanism of ET from Gd³⁺ to Ce³⁺ is found to be electric dipole-dipole interaction. The X-ray excited luminescence measurements show that the light yields of Ce³⁺ doped (Y, Gd)AGG samples increase from 5400 to 10000 ph/MeV with the gradual incorporation of Gd³⁺ ions, which is mainly owing to the ET from Gd³⁺ to Ce³⁺ ions. For Pr³⁺ doped (Y, Gd)AGG samples, the light yield values drop with Gd³⁺ incorporation, which may be caused by the presence of complex ET between Pr³⁺ 5d, 4f states and Gd³⁺ 4f-4f state.

Appendix A. Supplementary data

Supplementary data to this article can be found online at <https://doi.org/10.1016/j.jre.2020.01.001>.

References

- Blasse G, Bril A. A new phosphor for flying-spot cathode-ray tubes for color television: yellow-emitting Y₃Al₅O₁₂-Ce³⁺. *Appl Phys Lett*. 1967;11(2):53.
- Xia ZG, Meijerink A. Ce³⁺-doped garnet phosphors: composition modification, luminescence properties and applications. *Chem Soc Rev*. 2017;46(1):275.
- Qin X, Liu XW, Huang W, Bettinelli M, Liu XG. Lanthanide-activated phosphors based on 4f-5d optical transitions: theoretical and experimental aspects. *Chem Rev*. 2017;117(5):4488.
- Nakamura S. Present performance of InGaN-based blue/green/yellow LEDs. *Proc SPIE*. 1997;3002:26.
- Von Dollen P, Pimputkar S, Speck JS. Let there be light—with gallium nitride: the 2014 Nobel Prize in Physics. *Angew Chem, Int Ed*. 2014;53(51):13978.
- Kang TW, Park KW, Ryu JH, Lim SG, Yu YM, Kim JS. Strong thermal stability of Lu₃Al₅O₁₂:Ce³⁺ single crystal phosphor for laser lighting. *J Lumin*. 2017;191:35.

7. https://www.appotronics.com/alpd_tech.html#page4.
8. Ostermayer FW, Allen RB, Dierschke EG. Room-temperature cw operation of a GaAs_{1-x}P_x diode-pumped YAG:Nd laser. *Appl Phys Lett*. 1971;19(8):289.
9. Rosenkrantz LJ. GaAs diode-pumped Nd:YAG laser. *J Appl Phys*. 1972;43(11):4603.
10. Ronda C. *Luminescence: from theory to applications*. Weinheim: WILEY-VCH Press; 2008.
11. Dorenbos P. Fundamental limitations in the performance of Ce³⁺-, Pr³⁺-, and Eu²⁺-activated scintillators. *IEEE Trans Nucl Sci*. 2010;57(3):1162.
12. Li GG, Tian Y, Zhao Y, Lin J. Recent progress in luminescence tuning of Ce³⁺ and Eu²⁺-activated phosphors for pc-WLEDs. *Chem Soc Rev*. 2015;44(23):8688.
13. Xia ZG, Ma CG, Molokeev MS, Liu QL, Rickert K, Poeppelmeier KR. Chemical unit co substitution and tuning of photoluminescence in the Ca₂(Al_{1-x}Mg_x)(Al_{1-x}Si_{1+x}O₇):Eu²⁺ phosphor. *J Am Chem Soc*. 2015;137(39):12494.
14. Vrubel II, Polozkov RG, Shelykh IA, Khanin VM, Rodnyi PA, Ronda CR. Bandgap engineering in yttrium-aluminum garnet with Ga doping. *Cryst Growth Des*. 2017;17(4):1863.
15. Luo HD, Bos AJJ, Dorenbos P. Controlled electron-hole trapping and detrapping process in GdAlO₃ by valence band engineering. *J Phys Chem C*. 2016;120(11):5916.
16. Dorenbos P. Thermal quenching of Eu²⁺ 5d-4f luminescence in inorganic compounds. *J Phys Condens Matter*. 2005;17(50):8103.
17. Ueda J, Dorenbos P, Bos AJJ, Meijerink A, Tanabe S. Insight into the thermal quenching mechanism for Y₃Al₅O₁₂:Ce³⁺ through thermoluminescence excitation spectroscopy. *J Phys Chem C*. 2015;119(44):25003.
18. Nikl M, Mihóková E, Pejchal J, Vedda A, Fasoli M, Fontana I, et al. Scintillator materials – achievement, opportunities, and puzzles. *IEEE Trans Nucl Sci*. 2008;55(3):1035.
19. Fasoli M, Vedda A, Nikl M, Jiang C, Uberuaga BP, Stanek CR, et al. Band-gap engineering for removing shallow traps in rare earth Lu₃Al₅O₁₂ garnet scintillators with Ga³⁺ doping. *Phys Rev B*. 2011;84(8):081102.
20. Nazarov M, Noh DY. Rare earth double activated phosphors for different applications. *J Rare Earths*. 2010;28:1.
21. Zhou WJ, Gu M, Ou YY, Zhang CH, Zhang XJ, Liang HB, et al. Concentration-driven selectivity of energy transfer channels and color tunability in Ba₃La(PO₄)₃:Tb³⁺, Sm³⁺ for warm white LEDs. *Inorg Chem*. 2017;56(13):7433.
22. Kamada K, Endo T, Tsutsumi K. Composition engineering in cerium-doped (Lu,Gd)₃(Ga,Al)₅O₁₂ single-crystal scintillators. *Cryst Growth Des*. 2011;11(10):4484.
23. Kamada K, Yanagida T, Pejchal J, Nikl M, Endo T, Tsutsumi K, et al. Scintillator-oriented combinatorial search in Ce-doped (Y,Gd)₃(Ga,Al)₅O₁₂ multicomponent garnet compounds. *J Phys D: Appl Phys*. 2011;44(50):505104.
24. Ogino H, Yoshikawa A, Nikl M, Mares JA, Shimoyama J-I, Kishio K. Growth and optical properties of Lu₃(Ga,Al)₅O₁₂ single crystals for scintillator application. *J Cryst Growth*. 2009;311(3):908.
25. Prusa P, Kamada K, Nikl M, Yoshikawa A, Mares JA. Light yield of (Lu, Y, Gd)₃Al₂Ga₃O₁₂:Ce garnets. *Radiat Meas*. 2013;56:62.
26. Wu YT, Ding DZ, Pan SK, Yang F, Shi JY, Ren GH. The luminescence and energy transfer in Pr³⁺-Ce³⁺ co-doped Lu_{0.8}Sc_{0.2}BO₃ crystals. *J Lumin*. 2012;132(2):251.
27. Wu YT, Ren GH. Crystal growth, structure, optical and scintillation properties of Ce³⁺-doped Tb_{2.2}Lu_{0.8}Al₅O₁₂ single crystal. *CrystEngComm*. 2013;15(20):4153.
28. You FT, Zhang XG, Peng HS, Huang SH, Huang Y, Tao Y. Energy transfer and luminescent properties of Pr³⁺ and/or Dy³⁺ doped NaYF₄ and NaGdF₄. *J Rare Earths*. 2013;31(12):1125.
29. Nikl M, Kamada K, Kurosawa S, Yokota Y, Yoshikawa A, Pejchal J, et al. Luminescence and scintillation mechanism in Ce³⁺ and Pr³⁺ doped (Lu,Y,Gd)₃(Ga,Al)₅O₁₂ single crystal scintillators. *Phys Status Solidi C*. 2013;10(2):172.
30. Coelho AA. *Coelho software, Version 4*. Brisbane, Australia: Topas Academic; 2005.
31. Tao Y, Huang Y, Gao ZH, Zhang H, Zhou AY, Tan YL, et al. Developing VUV spectroscopy for protein folding and material luminescence on beamline 48B at the Beijing Synchrotron Radiation Facility. *J Synchrotron Radiat*. 2009;16(6):857.
32. Liu CM, Zhang S, Liu ZY, Liang HB, Sun SS, Tao Y. A potential cyan-emitting phosphor Sr₈(Si₄O₁₂)Cl₈:Eu²⁺ for wide color gamut 3D-PDP and 3D-FED. *J Mater Chem C*. 2013;1(7):1305.
33. Shi R, Huang Y, Tao Y, Dorenbos P, Ni HY, Liang HB. Luminescence and energy transfer between Ce³⁺ and Pr³⁺ in BaY₂Si₃O₁₀ under VUV-vis and X-ray excitation. *Inorg Chem*. 2018;57(14):8414.
34. Shannon RD. Revised effective ionic radii and systematic studies of interatomic distances in halides and chalcogenides. *Acta Crystallogr - Sect A Cryst Phys Diffr Theor Gen Crystallogr*. 1976;32(5):751.
35. Blasse G, Bril A. Investigation of some Ce³⁺-activated phosphors. *J Chem Phys*. 1967;47(12):5139.
36. Chewpraditkul W, Panek D, Bruza P, Chewpraditkul W, Wanarak C, Nikl M, et al. Luminescence properties and scintillation response in Ce³⁺-doped Y₂Gd₁Al_{5-x}Ga_xO₁₂ (x = 2, 3, 4) single crystals. *J Appl Phys*. 2014;116(8):083505.
37. Dorenbos P. Electronic structure and optical properties of the lanthanide activated RE₃(Al_{1-x}Ga_x)₅O₁₂ (RE = Gd, Y, Lu) garnet compounds. *J Lumin*. 2013;134:310.
38. Dorenbos P. Charge transfer bands in optical materials and related defect level location. *Opt Mater*. 2017;69:8.
39. Ueda J, Tanabe S. Review of luminescent properties of Ce³⁺-doped garnet phosphors: new insight into the effect of crystal and electronic structure. *Opt Mater*. X. 2019;1:100018.
40. Dorenbos P. Determining binding energies of valence-band electrons in insulators and semiconductors via lanthanide spectroscopy. *Phys Rev B*. 2013;87(3):035118.
41. Dorenbos P. Valence stability of lanthanide ions in inorganic compounds. *Chem Mater*. 2005;17(25):6452.
42. Ueda J, Maki R, Tanabe S. Vacuum referred binding energy (VRBE)-guided design of orange persistent Ca₃Si₂O₇:Eu²⁺ phosphors. *Inorg Chem*. 2017;56(17):10353.
43. Liu CM, Qi ZM, Ma CG, Dorenbos P, Hou DJ, Liang HB, et al. High light yield of Sr₈(Si₄O₁₂)Cl₈:Eu²⁺ under X-ray excitation and its temperature-dependent luminescence characteristics. *Chem Mater*. 2014;26(12):3709.
44. Ogiegio JM, Katelnikovas A, Zych A, Jüstel T, Meijerink A, Ronda CR. Luminescence and luminescence quenching in Gd₃(Ga, Al)₅O₁₂ scintillators doped with Ce³⁺. *J Phys Chem A*. 2013;117(12):2479.
45. Ueda J, Dorenbos P, Bos AJJ, Kuroishi K, Tanabe S. Control of electron transfer between Ce³⁺ and Cr³⁺ in the Y₃Al_{5-x}Ga_xO₁₂ host via conduction band engineering. *J Mater Chem C*. 2015;3(22):5642.
46. Song Z, Xia ZG, Liu QL. Insight into the relationship between crystal structure and crystal-field splitting of Ce³⁺ doped garnet compounds. *J Phys Chem C*. 2018;122(6):3567.
47. Skaudzius R, Katelnikovas A, Ensling D, Kareiva A, Jüstel T. Dependence of the 5D₀→7F₄ transitions of Eu³⁺ on the local environment in phosphates and garnets. *J Lumin*. 2014;147:290.
48. Asami K, Ueda J, Kitaura M, Tanabe S. Investigation of luminescence quenching and persistent luminescence in Ce³⁺ doped (Gd, Y)₃(Al, Ga)₅O₁₂ garnet using vacuum referred binding energy diagram. *J Lumin*. 2018;198:418.
49. Inokuti M, Hirayama F. Influence of energy transfer by the exchange mechanism on donor luminescence. *J Chem Phys*. 1965;43(6):1978.
50. Liang HB, Lin HH, Zhang GB, Dorenbos P, Su Q. Luminescence of Ce³⁺ and Pr³⁺ doped Sr₂Mg(BO₃)₂ under VUV-UV and X-ray excitation. *J Lumin*. 2011;131(2):194.
51. Ueda J, Meijerink A, Dorenbos P, Bos AJJ, Tanabe S. Thermal ionization and thermally activated crossover quenching processes for 5d-4f luminescence in Y₃Al_{5-x}Ga_xO₁₂:Pr³⁺. *Phys Rev B*. 2017;95(1):014303.
52. Zhou WJ, Hou DJ, Pan FJ, Zhang BB, Dorenbos P, Liang HB, et al. VUV-vis photoluminescence, X-ray radioluminescence and energy transfer dynamics of Ce³⁺ and Pr³⁺ doped LiCaBO₃. *J Mater Chem C*. 2015;3(35):9161.
53. Blasse G, Grabmaier B. *Luminescent materials*. Berlin: Springer Verlag; 1994.